

Mapping the low surface brightness Universe in the UV band with Ly α emission from IGM filaments

Marta B. Silva¹ *, Robin Kooistra¹, Saleem Zaroubi¹ ²

Kapteyn Astronomical Institute, University of Groningen, Landleven 12, 9747AD Groningen, the Netherlands

Department of Natural Sciences, The Open University of Israel, 1 University Road, P.O. Box 808, Ra'anana 4353701, Israel

8 October 2018

ABSTRACT

A large fraction of the baryonic matter in the Universe is located in filaments in the intergalactic medium. However, the low surface brightness of these filaments has not yet allowed their direct detection except in very special regions in the circum-galactic medium (CGM).

Here we simulate the intensity and spatial fluctuations in Lyman Alpha (Ly α) emission from filaments in the intergalactic medium (IGM) and discuss the prospects for the next generation of space based instruments to detect the low surface brightness universe at UV wavelengths. Starting with a high resolution N-body simulation we obtain the dark matter density fluctuations and associate baryons with the dark matter particles assuming that they follow the same spatial distribution. The IGM thermal and ionization state is set by a model of the UV background and by the relevant cooling processes for a hydrogen and helium gas. The Ly α emissivity is then estimated, taking into account recombination and collisional excitation processes. We find that the detection of these filaments through their Ly α emission is well in the reach of the next generation of UV space based instruments and so it should be achieved in the next decade. The density field is populated with halos and galaxies and their Ly α emission is estimated. Galaxies are treated as foregrounds and so we discuss methods to reduce their contamination from observational maps. Finally, we estimate the UV continuum background as a function of the redshift of the Ly α emission line and discuss how this continuum can affect observations.

Key words: ultraviolet: general, galaxies: general — intergalactic medium, cosmology: theory — diffuse radiation — large scale structure of universe

1 INTRODUCTION

Galaxies and galaxy clusters are connected by filamentary structures known as the cosmic web. A large fraction of the baryonic matter is located in these low density filaments which are characterized by a very low surface brightness. Observing and mapping these baryons is an important step in order to complete our understanding of the mechanisms involved in galaxy formation and evolution at large scales as well as to correctly model interactions and clustering of galaxies. Also, the cold gas in these filaments will eventually flow into galaxies and be involved in processes of stellar formation and therefore its important to accurately model its thermal state.

While the CGM can be probed with metal lines such as OVI and CIV (Furlanetto et al. 2004; Keating et al. 2014; Liang et al. 2015), lower density regions of the IGM have a much smaller metallicity and can only be probed through hydrogen or helium transition lines. At high redshifts neutral gas in the IGM is of-

ten detected through observations of Ly α absorption features in the spectra of quasars (Gunn & Peterson 1965) or through observations of Ly α blobs, which are spatially extended Lyman alpha nebulae in the densest regions of the Universe. At lower redshifts the gas, however is more ionized and so the scattering of Ly α photons is reduced. Searches for Ly α blobs at $z \sim 0.8$ with GALEX (The Galaxy Evolution Explorer) have so far not been successful, which might indicate that these structures are restricted to the high redshift universe (Keel et al. 2009).

Also, Ly α emission originating at a redshift of $z \lesssim 2.2$ has to be detected from space, because the Earth's atmosphere is opaque to UV radiation. At low redshifts the neutral gas is therefore mostly probed by radio observations of HI 21 cm absorption features. Current radiotelescopes can only probe this line at $z \lesssim 0.6$, although in the far future the SKA-2 experiment will be able to go much higher in redshift.

The hydrogen Ly α line is usually the strongest emission line in galaxy spectra with an intrinsic flux proportional to the ionizing photons emissivity. This is also a promising line to probe the IGM, where it is usually the main cooling mechanism.

*E-mail: silva@astro.rug.nl

Lyman alpha emission is usually associated with ionized recombining gas and in the cold IGM its intensity is mainly set by the thermal and ionization state of the gas which are related to the UV and X-ray backgrounds. The maximum Ly α intensity in regions powered by the UV/X-ray backgrounds is about 50% of the intensity of this ionizing radiation and can therefore be used to constrain it. In the overdense CGM, most of the gas, however is shock heated and collisional excitation is the main mechanism leading to Ly α emission (Furlanetto et al. 2003, 2005; Davé et al. 2010). The fraction of the gas that is shock-heated increases towards lower redshift but should be smaller than the cold gas fraction, even in the local universe Davé et al. (2010). Currently, gas filaments in the IGM are mostly indirectly detected through optical observations of the stars and galaxies they contain. A direct detection of a large gas filament surrounding a quasar was recently reported by Cantalupo et al. (2014) at $z \sim 2.3$. The Ly α emission in this filament is powered by UV emission from a local quasar. Thus, its intensity is much larger than the expected UV background powered emission. Also, it is likely that this filament is at a density peak which is further boosting its Ly α emission.

Here, we propose to use intensity mapping of the Ly α line from the local universe to $z \sim 3$ as a probe of the IGM baryonic content and of the astrophysical properties of IGM filaments. The main objective is to detect and characterise the faint emission from UV/X-ray background powered filaments. Additionally, with these maps we aim to probe the UV background intensity, since the maximum Ly α emissivity from IGM filaments occurs in optically thick regions and should therefore have roughly half of the intensity of this background.

Intensity maps will mainly provide statistical quantities such as the intensity and power spectrum of the signal, with the advantage that for this it is not required for the signal to be above the instrumental noise, such as in the case of galaxy surveys.

The possibility of mapping Ly α emission in the optical band at $z = 3$ has already been discussed in Furlanetto et al. (2005) and Martin et al. (2014). In the UV band, most studies of this transition are focused on the prospects for mapping Lyman alpha absorbers identified by the mean flux decrement along galaxy lines of sight (see eg. Davé et al. (2010)) and do not consider the possibility of detecting Ly α emission in the IGM, since it was not seen as an attainable possible goal in the foreseeable future. The problem resides mainly in the technical difficulties in measuring UV radiation, while successfully removing the galactic and extragalactic contamination. Fortunately, new technological advances make Ly α intensity mapping in the UV an achievable goal in the next decade. Therefore, in this study, we use updated astrophysical and cosmological parameters to estimate the Ly α signal from the IGM. In particular, estimates are shown for the required sensitivity, field-of-view and resolution to measure the bulk of the signal and to detect the power spectra of Ly α emission fluctuations.

Our study shows that any high sensitivity galaxy survey in the UV band will also be sensitive to emission from gas filaments. Even if the overall Ly α emission from galaxies is much higher than the emission from filaments, the effective escape fraction of Ly α photons from galaxies at $z \simeq 3.0$ is quite small and so it will push towards increasing the new UV instruments, sensitivity. Conversely, the Ly α escape fraction of filaments is close to unity, which makes them easier to observe.

This paper is organized as follows. The model and the simulations used to obtain maps of the ionization and thermal state of the IGM are presented in Section 2. In Section 3 the processes leading to Ly α emission from galaxies and from the IGM are dis-

cussed and predictions for the overall intensities are presented. In Section 4 the main results are shown, including several maps obtained from the simulation and the several relevant Ly α emission power spectra. The experimental setup necessary for measuring the target emission is presented in Section 5. In Section 6 the modeling of the contaminants in Ly α emission intensity maps is introduced and foreground removal techniques are discussed. Finally, the main results and conclusions are presented in Section 7.

2 MODELING THE THERMAL AND IONIZATION STATE OF THE IGM

Direct detection of IGM filaments through observations of emission/absorption by transition lines will make it possible to properly map the thermal and ionization state of the IGM gas, which can be used to constrain the UV/X-ray background originating in the overall emissivity from quasars and stars through time. At the relevant redshifts for this study, this background is dominated by emission from quasars and so the proposed observations will mainly put constraints on the overall quasar luminosity density and, in particular, on the poorly constrained low energy end of the quasars emission spectra.

We employ the Gadget 2 N-body code to obtain a dark matter (DM) only simulation (Springel et al. 2001; Springel 2005) using the best fit cosmological parameters from Planck + WMAP (Planck Collaboration et al. 2014) ($\Omega_b h^2 = 0.022032$, $h = 0.6704$, $Y_P = 0.2477$, $n_s = 0.9619$ and $\sigma_8 = 0.8347$) and save the outputs correspondent to redshifts 0 to 3.

The simulated volume is $50 \text{ Mpc}^3/h^3$ with a $10^7 M_\odot$ mass resolution. The cloud in cell (CIC) method is then used to distribute the particles in 3D boxes with $N = 800^3$ cells. In this study we assume that the baryon spatial distribution follows that of the dark matter particles.

The temperature and ionizing state of the gas in each cell of the simulation were modeled, assuming ionizing and thermal equilibrium set by the ionizing background radiation, adiabatic cooling, and all the heating, recombination and collisional processes relevant for a hydrogen and helium gas. The temperature of the gas was obtained with

$$\frac{dT_{\text{gas}}}{dt} = -2H(z)T_{\text{gas}} + \frac{2}{3} \frac{\mathcal{H} - \Lambda}{nk_B}, \quad (1)$$

where \mathcal{H} and Λ are respectively the heating and cooling functions and n is the baryon number density.

The adiabatic cooling was computed assuming only the average Hubble expansion and neglecting peculiar velocities and we are therefore underestimating it. Peculiar velocities dominate the gas expansion at low scales. However, at the large scales relevant for this study these velocities are smoothed enough that, for overdensities of 10 - 20 times the average gas density, the peculiar velocity gradients are on average a few times lower than the average Hubble expansion. For more details see (Kooistra et al. in prep). We did not account for metal cooling given the expected low metallicity of IGM filaments and the low temperatures involved.

We used the Haardt & Madau (2012) UV/X-ray background model, which includes the integrated emissivity from star forming galaxies and active galactic nuclei (AGN), as a source of heating and ionizing photons. This model assumes a relatively small escape fraction of ionizing photons from star forming galaxies and therefore there is a good chance that it is underestimating this emission. However, at $z < 3$ the predicted background is dominated by AGN

emission and so we will not discuss the uncertainties in this part of the model further.

The AGN background radiation predicted by this model is based on the few available observational results of AGN number counts and spectral emissivities. Attenuation of this background by absorption in gas clouds in the IGM is also taken into account, based on observations of Ly α forest features in the spectra of background sources.

There is a large uncertainty in the modelling of the AGN background radiation due to the poorly known number density of AGN as we go to higher redshifts and due to the lack of measurements of AGN emissivity at UV wavelengths. The resulting uncertainty in the UV/X-ray background is therefore of at least one order of magnitude and increases towards lower redshifts. However, the impact of this uncertainty in the gas ionization and thermal state, and therefore in the total Ly α emissivity from IGM filaments, will be of a factor of 2 or 3 at most.

At $z < 3$, and especially as we approach $z = 0$, the attenuation length is high enough that there are several sources contributing to the flux arriving at each point of the IGM and so it is fair to assume a spatially homogeneous UV background (Meiksin 2009). For the cold IGM, we can assume that the heating and the ionization state of gas filaments is set by the UV/X-ray background. However, in the vicinity of a young galaxy or an active galactic nucleus, the gas will be hotter and more ionized and so the equilibrium assumptions will not hold.

Also, shock-heating of gas during gravitational collapse of matter is increasingly important towards lower redshifts. This code does not account for shock-heating of gas, metal cooling or self-shielding of overdense gas. The correct modeling of these processes requires very high resolution hydrodynamical simulations which would restrict this study to low volumes, which is not our objective since we mainly propose to probe the large scale structure distribution of gas and the location of the baryons in the cold IGM. For that we need relatively large volumes and do not need to properly resolve the complex processes involved in setting the temperature and ionization state of the gas in the CGM. Nevertheless, even in the local Universe most of the IGM baryons are likely to be located in cold gas filaments Davé et al. (2010). For more precise hydrodynamic simulations of Ly α emission/absorption in the IGM we refer the reader to the study of fluorescent Ly α emission by Kollmeier et al. (2010) which mainly targets emission from $z \sim 2 - 3$. Another useful reference to which we compare some of our results is the study by Davé et al. (2010), who simulated IGM Ly α absorbers in a volume of $48 \text{ Mpc}^3/h^3$ from $z \sim 0 - 2$ with the main objective of predicting the number of Ly α absorbers detectable using the Hubbles Cosmic Origins Spectrograph.

The distribution of hydrogen in galaxies and in the IGM as a function hydrogen density is shown in Figure 1. This figure shows that a large fraction of the baryonic matter is located in IGM filaments and so it illustrates the importance of observing this filaments.

3 MODELING LYMAN ALPHA EMISSION

In this section, we describe the essential assumptions of our modeling of Ly α emission from the IGM and from galaxies and then in Section 4 we present our simulation analysis and main results.

Lyman alpha photons are emitted by hydrogen during recombinations or due to collisional excitations between neutral hydrogen and free electrons. Both of these processes are usually pow-

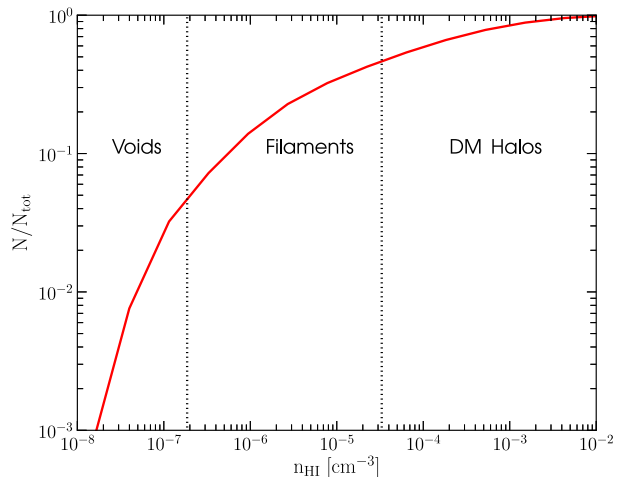


Figure 1. Cumulative distribution of hydrogen baryons as a function of matter overdensity at $z = 0.65$.

ered by UV/X-ray emission from stars or quasars. The additional Ly α emission, powered by the energy released during gravitational collapse, is mostly relevant for studies of the CGM and so it can be safely ignored in this study. On the other hand, an additional source of Ly α photons would only increase the detectability of the proposed target signal.

3.1 Lyman alpha emission from the IGM

Lyman alpha emission naturally traces the more overdense regions of the gas where the recombination and excitation rates for hydrogen are higher, which in the IGM corresponds to the overdense gas filaments. The intensity of Ly α emission in these filaments depends on their density, ionization and thermal state. The luminosity density (per comoving volume) in Ly α emission from hydrogen recombinations in the IGM, $\ell_{\text{rec}}^{\text{IGM}}$ is

$$\ell_{\text{rec}}^{\text{IGM}}(z) = f_{\text{rec}} \dot{n}_{\text{rec}} E_{\text{Ly}\alpha}, \quad (2)$$

where the probability of emission of a Ly α photon per recombination of a hydrogen atom is

$$f_{\text{rec}}^{\text{A}} = 0.41 - 0.165 \log_{10}(T_{\text{K}}/10^4 \text{K}) - 0.015(T_{\text{K}}/10^4 \text{K})^{-0.44}. \quad (3)$$

This relation is taken from Dijkstra (2014) and is appropriate for $100 \text{ K} < T_{\text{K}} < 10^5 \text{ K}$ and for a case A recombination coefficient. The number density of recombinations per second, \dot{n}_{rec} , is given by:

$$\dot{n}_{\text{rec}}(z) = \alpha_{\text{A}} n_{\text{e}}(z) n_{\text{HII}}(z), \quad (4)$$

where $n_{\text{HII}} = x_i \frac{n_{\text{b}}(1-Y_{\text{p}})}{1-3/4Y_{\text{p}}}$ is the ionized hydrogen number density (x_i is the mass averaged ionized fraction, n_{b} the baryon comoving number density) and the free electron density can be approximated by $n_{\text{e}} = x_i n_{\text{b}}$. In the IGM, the gas is mostly optically thin and so the recombination probability was modeled with the case A recombination coefficient taken from Fukugita & Kawasaki (1994)

$$\begin{aligned} \alpha_{\text{A}} &\approx 6.28 \times 10^{-11} T_{\text{K}}^{-0.5} (T_{\text{K}}/10^3 \text{K})^{-0.2} \\ &\times [1 + (T_{\text{K}}/10^5 \text{K})^{0.7}]^{-1} \text{ cm}^3 \text{ s}^{-1}. \end{aligned} \quad (5)$$

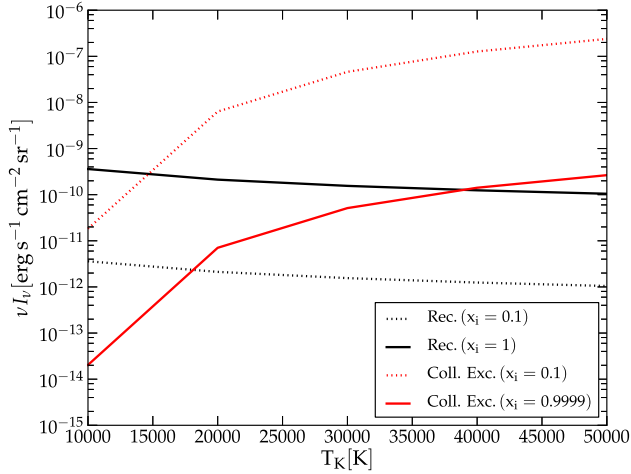


Figure 2. Theoretical intensity of Ly α emission from recombinations and collisions in the IGM. Recombination emission was estimated assuming full ionization of the gas, whereas collisional emission was estimated for different values of x_i . The intensities shown assume a clumping factor of 1 and can be easily scaled to higher clumping factors just by multiplying the resulting intensity by C.

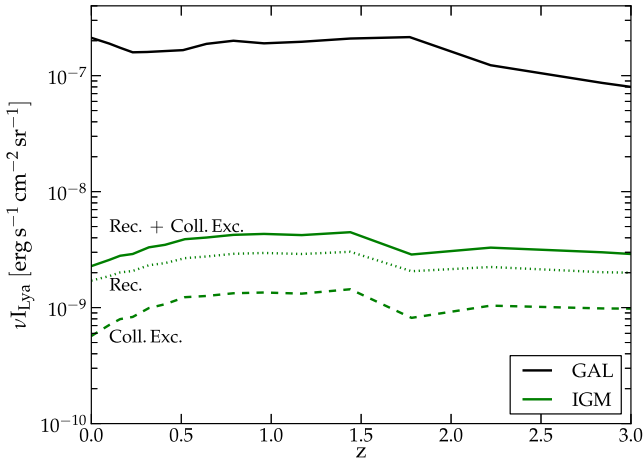


Figure 3. Lyman alpha intensity from galaxies and the IGM as a function of redshift obtained from the simulations.

Using a case B recombination rate would result in a smaller number of recombinations but a higher probability of Ly α photon emission per recombination. Therefore, the overall emission rate of Ly α photons has a weak dependence on the choice of recombination coefficient (Dijkstra 2014). The luminosity density (per comoving volume) in Ly α emission from collisional excitation of neutral hydrogen by free electrons in the IGM is

$$\ell_{\text{exc}}^{\text{IGM}}(z) = n_e n_{\text{HI}} q_{\text{Ly}\alpha} E_{\text{Ly}\alpha}, \quad (6)$$

where $q_{\text{Ly}\alpha}$ is the effective collisional excitation coefficient which is calculated as in Silva et al. (2013).

Figure 2 shows the theoretical estimate of the Ly α intensity from the IGM at $z = 0.65$, as a function of gas temperature. This figure shows that while in cold IGM filaments Ly α emission is

mainly originated in recombinations in the WHIM collisions will be the main source of Ly α photons and the Ly α intensity will be higher by a few orders of magnitude.

Figure 3 shows the same intensity taken from our simulations but as a function of redshift. From the simulations, the Ly α emission mainly originates in recombinations from gas with a clumping factor of ~ 5 and $T_{\text{K}} \sim (1 - 2) \times 10^4$ K and has an intensity of $\nu I_{\text{Ly}\alpha}(z = 0.65) \sim 2 \times 10^{-9}$ erg s $^{-1}$ cm $^{-2}$ sr $^{-1}$. Figure 3 also shows that galaxies are likely to be the dominant source of Ly α emission. Small variations in our estimates of the thermal and ionization state of the gas might lead to an increase (by a factor of a few) of the intensity of Ly α emission from collisional excitations, but will have little impact on the Ly α recombination emission. By using simulations we were able to determine the ionization and thermal state of the gas for each cell of the simulation. This is an improvement over the generalized use of a fixed temperature or the use of a temperature parameterized by a power law with a fixed exponent (the adiabatic index), which is only appropriate for low density gas ($\delta < 10$) cooling adiabatically. Also, the current uncertainty in the adiabatic index is relatively high ($1.3 > \gamma > 1.6$) Schaye et al. (2000); Lidz et al. (2010); Becker et al. (2011), which results in a considerable change in the intensity and spatial distribution of the Ly α emission.

3.2 Lyman alpha emission from Galaxies

In galaxies the main process leading to Ly α emission is recombinations. This Ly α emissivity can be roughly estimated as:

$$\dot{N}_{\text{Ly}\alpha}^{\text{rec}} = A_{\text{He}} \dot{N}_{\text{ion}} (1 - f_{\text{esc}}) f_{\text{rec}} f_{\text{esc}}^{\text{Ly}\alpha}. \quad (7)$$

Here, \dot{N}_{ion} is the rate of emission of ionizing photons by the galaxy, A_{He} is a correction factor that accounts for the photons spent in the ionization of helium, f_{rec} accounts for the fraction of recombinations that result in the emission of a Ly α photon; $f_{\text{esc}}^{\text{Ly}\alpha}$ corresponds to the fraction of Ly α photons that escape the galaxy into the IGM and f_{esc} is the fraction of ionizing photons that escape the galaxy without being absorbed by dust.

We assume f_{esc} to be around 20% as predicted by Yajima et al. (2014) using cosmological hydrodynamical simulations and a state of the art radiative transfer code. For low redshift studies the Ly α luminosity is usually estimated assuming $f_{\text{esc}} = 0$, which is a reasonable approximation in most cases, since the fraction of radiation escaping galaxies scales inversely with the galaxy dust content and so on average decreases towards low redshifts and high masses, which are the systems that are more easily observed. Also, the uncertainty in f_{esc} is very high given the very small number of direct observational constraints and the large variation of the measured value for different lines of sight.

The amount of Ly α photons emitted due to collisional excitation of neutral hydrogen by free electrons is proportional to the leftover energy released into the gas during hydrogen ionizations and thus depends on the hardness of the stellar spectrum. The number of Ly α collisional excitations is

$$\dot{N}_{\text{Ly}\alpha}^{\text{exc}} = A_{\text{He}} \dot{N}_{\text{ion}} (1 - f_{\text{esc}}) f_{\text{exc}} f_{\text{esc}}^{\text{Ly}\alpha} E_{\text{exc}} / E_{\text{Ly}\alpha} \quad (8)$$

where following the formalism described in (Gould & Weinberg 1996) and estimating the average energy of an ionizing photon using the spectral energy distribution (SED) of galaxies from the Maraston (2005) models, we obtained $E_{\text{exc}} \sim 2.14$ eV, for the

leftover energy per recombination, in a galaxy powered by star formation. The emission rate of ionizing photons from galaxies can be estimated from the galaxy SFR as:

$$\dot{N}_{\text{ion}} = Q_{\text{ion}} \times \text{SFR}, \quad (9)$$

where Q_{ion} is the average number of ionizing photons emitted per solar mass in star formation, which at solar metallicity and for a Salpeter mass function is given by $2.36 \times 10^{60} M_{\odot}^{-1}$ (Shull et al. 2012). The resulting intensity of Ly α emission from galaxies is

$$\begin{aligned} I_{\text{Ly}\alpha}^{\text{GAL}} &= E_{\text{Ly}\alpha} \dot{N}_{\text{Ly}\alpha} \\ &\approx 1.55 \times 10^{42} (1 - f_{\text{esc}}) f_{\text{esc}}^{\text{Ly}\alpha} \frac{\text{SFR}}{M_{\odot} \text{ yr}^{-1}} \text{erg s}^{-1}. \end{aligned} \quad (10)$$

We assume that the fraction of Ly α photons which are not absorbed by dust in the ISM is of the order of $f_{\text{esc}}^{\text{Ly}\alpha} = 0.3$, which is the average value for $z < 3$ also obtained by (Yajima et al. 2014). This is the appropriate value for intensity mapping studies, since it accounts for the fraction of Ly α photons that escape from galaxies and does not account for scattering or absorption of Ly α photons in the IGM, since these processes conserve the number of photons and therefore the Ly α intensity signal as measured by an intensity mapping experiment. The much smaller value usually stated in observational studies refers to the effective escape fraction of Ly α photons, which basically considers that Ly α photons are lost when scattered out of the line of sight, since these photons will no longer be detected by an observation with a small field of view aiming to resolve an individual source (Hayes et al. 2011; Dijkstra & Jeeon-Daniel 2013).

We use the halo finder in the Simfast21 code described in (Santos et al. 2010; Silva et al. 2012) to extract the DM halos from the N-body simulation. We then estimate their associated star formation rate and finally their Ly α emission. The halos mass is converted into a star formation rate using the relation between these quantities found in the Guo et al. (2011) and De Lucia & Blaizot (2007) galaxy catalogs obtained by post processing, respectively, the outputs from the Millennium II (Boylan-Kolchin et al. 2009) and Millennium I (Springel et al. 2005) dark matter simulations. For the mass range available, the parameterizations of the SFR versus halo mass relations were adjusted to fit the observationally based constraints from Popping et al. (2015) and the simulations from Behroozi et al. (2013). However, we note that this correction had a small impact in the final results.

4 LYMAN ALPHA INTENSITY MAPS AND POWER SPECTRUM

In the first part of this section the main results from the simulations, the maps of Ly α emission, are presented assuming experimental setups with different sensitivities. These maps can therefore be used to determine the experimental setup required to successfully detect the IGM Ly α signal. We also present a power spectrum analysis of the simulation results.

4.1 Lyman alpha intensity results

Figure 4 shows the intensity fluctuations in Ly α emission from galaxies and from the IGM, and how they correlate with the peaks in the HI density. This figure illustrates how an intensity mapping experiment targeting IGM emission would be able to trace many

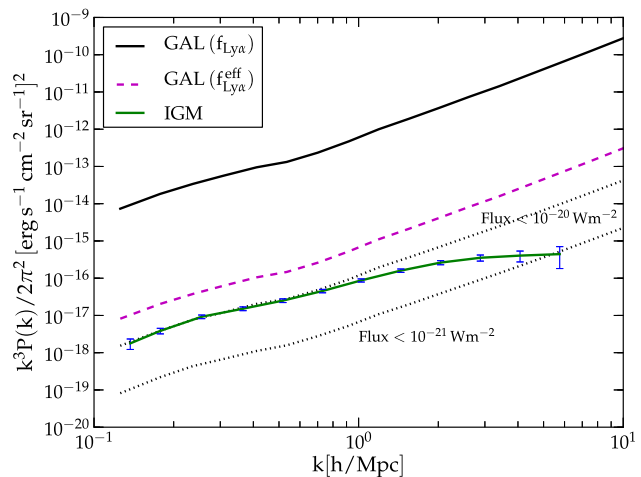


Figure 5. Power spectra of Ly α emission from galaxies and from the IGM at $z = 0.65$. The black lines account only for dust absorption of Ly α photons in the galaxies ISM while the magenta dashed line also accounts for scattering/absorption of Ly α photons in the IGM. The black dotted lines assume only emission from galaxies with Ly α fluxes below $10^{-20} \text{ W m}^{-2}$ and $10^{-21} \text{ W m}^{-2}$. The error bars correspond to the experimental setup of the fiducial instrument described in Section 5.1.

more structures than an instrument targeting only galaxies. The bottom four panels in Figure 4 show the structures observed by experiments with decreasing sensitivities. From these panels we can predict that observing the main filamentary structures in the IGM through their Ly α emission requires an experiment with a sensitivity of the order of $\nu I_{\text{Ly}\alpha} = 10^{-9} \text{ erg s}^{-1} \text{ cm}^{-2} \text{ sr}^{-1}$. This intensity corresponds approximately to the intensity of Ly α emission from IGM filaments assuming the (Haardt & Madau 2012) UV background model. Given the uncertainties in this model, we multiplied this background by a factor of two and found that the Ly α intensity would only increase by about 20%, which would have a minimum impact on our results.

This intensity can be converted to relative magnitudes using the formula from Oke & Gunn (1983) given by:

$$m = -48.6 - 2.5 \log f_{\nu}. \quad (11)$$

with magnitudes in units of mag/arcsec^2 and fluxes in units of $\text{erg s}^{-1} \text{ cm}^{-2} \text{ Hz}^{-1} \text{ arcsec}^{-2}$. Therefore, a surface brightness of 37 mag/arcsec^2 in the UV band corresponds to a Ly α intensity of $\nu I_{\text{Ly}\alpha} = 3.66 \times 10^{-9} \text{ erg s}^{-1} \text{ cm}^{-2} \text{ sr}^{-1}$.

Figure 5 shows that, at $z = 0.65$, the predicted power spectra of Ly α emission from galaxies is orders of magnitude higher than that of emission from the IGM. Furthermore, Figure 6 shows that this difference is maintained throughout the relevant redshift range. Since the objective of this study is the detection of Ly α emission from the IGM we treat Ly α emission from galaxies as a foreground and determined what fraction of the observational maps need to be masked in order to successfully extract the IGM signal. From our simulations we estimate that, for this to be possible, we need to mask galaxies with Ly α fluxes above ($10^{-20} - 10^{-21} \text{ W m}^{-2}$), which corresponds to a number density of masked galaxies of $\sim 0.11 - 0.22 \text{ Mpc}^{-3}$, assuming the experimental setup proposed in Section 5.1. In Figure 5 we show the contamination power spectra before and after the masking technique is applied. As can be observed in this figure, the galaxy power spectrum suffers from a

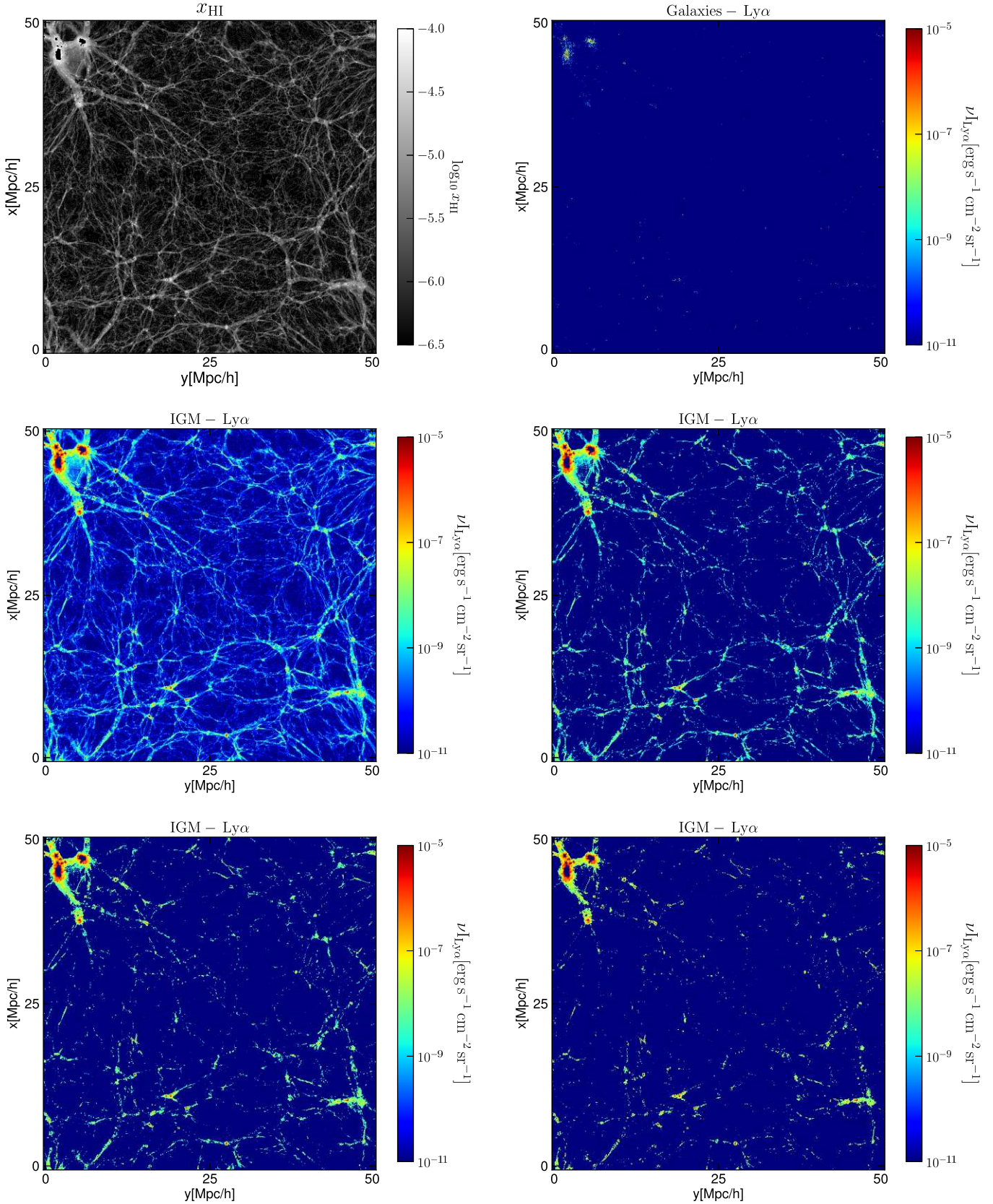


Figure 4. Simulated maps at $z = 0.65$. Left upper panel: HI fraction in the IGM. Right upper panel: Lyman alpha intensity from galaxies. Except in this panel, galaxies are presented as dark regions, since we start by ignoring the properties from these regions. Middle and lower panels show the intensity of Lyman alpha emission from recombinations and collisional excitations in the IGM. These panels from top to bottom and from left to right assume the full $\text{Ly}\alpha$ signal, and the $\text{Ly}\alpha$ signal above an intensity cut of $(0.58, 1.46, 3.66) \times 10^{-9} \text{ erg s}^{-1} \text{ cm}^{-2} \text{ sr}^{-1}$, respectively. These intensity cuts correspond to flux sensitivities of (39, 38, 37) mag/arcsec² in the UV band, respectively.

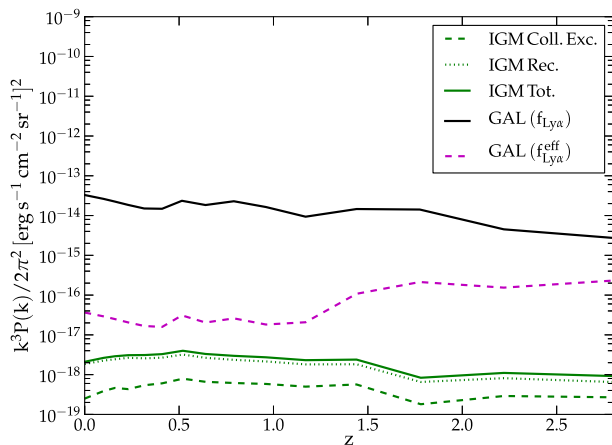


Figure 6. Power spectra of Ly α emission from galaxies and from the IGM at $k = 0.177 \text{ h/Mpc}$.

large shot noise contribution at $k \gtrsim 0.06$, which makes it easy to distinguish from the power spectrum of IGM fluctuations. The shape of the observed power spectra can therefore be used to confirm if enough low luminosity galaxies were masked and thus if we are indeed detecting the signal from the IGM.

5 EXPERIMENTS FOR DETECTING UV LYMAN ALPHA EMISSION

Currently, there are few experiments probing Ly α emission/absorption in the UV regime and these missions mainly target strong emission from galaxies or from the WHIM. The low surface brightness emission at UV wavelengths is, however, essential to probe galaxies at the epoch of peak SFR activity ($z \sim 2$) which is pushing the sensitivity of UV instruments to increasingly lower fluxes and will bring them to the level necessary to also probe Ly α emission from IGM filaments. Probing the low surface brightness universe is limited by systematics, sky variability, straylight, flat field accuracy and extended PSF wings and only now, with the advent of technological advances, is this goal becoming possible.

Examples of current or proposed experiments that propose to probe IGM emission include the following missions. The Faint Intergalactic Redshifted Emission Ballon (FIREBall2) is able to measure Ly α , OVI and CIV emission from the WHIM at 205 nm (Tuttle et al. 2010), and its successor, the proposed Imaging Space Telescope for Origins Survey (ISTOS) plans on targeting Ly α emission from $z \sim 0.5 - 1.2$. There are also several orbital sounding rockets carrying integral field spectrometers able to detect Ly α emission from galaxies and from the CGM in the redshift range ($z \sim 0 - 1.5$) (France et al. 2015). The Cosmic Origins Spectrograph (COS) on board of the Hubble Space Telescope also targets Ly α emission from galaxies and from the CGM in the redshift range ($z \sim 0 - 1.5$) (Morse et al. 1998; Green et al. 2003).

These experiments will, however, not be able to detect the faint population of Ly α emitters or the cold IGM. On the other hand, the recently proposed Messier satellite plans to achieve unprecedented surface brightness levels of 37 mag/arcsec^2 in the UV, which is enough to probe emission from faint galaxies, from the WHIM and even from the cold IGM. This satellite will carry a photometer with

a very high spatial resolution but with mostly broadband frequency filters. The main sensitivity of the satellite will be at $z \sim 0.65$, since it will have a narrow band filter centered at 200 nm. The proposed frequency band of $\Delta\lambda \sim 50 \text{ nm}$, however, is too large to identify IGM filaments, although it will be sensitive to the overall emission from several filaments. We note that the width of IGM filaments should be of the order of 0.5 Mpc/h (Tempel et al. 2014).

5.1 Experimental setup for Lyman Alpha emission Intensity Mapping

In this section we describe the experimental setup of a UV satellite capable of detecting and mapping Ly α emission from IGM filaments and thus also able to probe the low surface brightness universe. The setup of the described detector is appropriate, not only to detect this signal, but also to study the statistical properties and the spatial distribution of IGM filaments. If we just aim at detecting the filaments, an experiment with a smaller resolution would suffice.

We take a UV sensitivity of 37 mag/arcsec^2 as the minimum surface brightness level required to detect most ($> 90\%$) of the emission from faint filaments in the IGM at $z = 0.65$, as estimated in Section 4.1. This UV magnitude corresponds to the detection of Ly α emission above $\nu I_{\text{Ly}\alpha} \sim 3.7 \times 10^{-9} \text{ erg s}^{-1} \text{ cm}^{-2} \text{ sr}^{-1}$.

A lower sensitivity would still allow the detection of many IGM filaments. However, since we propose to analyze these filaments at a statistical level, using their intensity and power spectra, the more filaments we can detect the more we can say about their properties.

Given the length of up to 60 Mpc/h of the filaments recently identified by Tempel et al. (2014) in the SDSS public galaxies catalog, we assume the minimum area to be observed by the proposed experiment to be of 60 Mpc/h , which at $z \sim 0.65$ requires at least a $2^\circ \times 2^\circ$ observational field of view. The ideal spatial resolution necessary to identify the filaments is of the order of 1 Mpc . Lower resolutions would however still allow for the statistical detection of this signal, but would make the masking of foreground emission very difficult. This spatial resolution corresponds to a frequency resolution of $R=1000$ and an angular resolution of $85''$. A telescope with an 80 cm aperture and 200×200 elements could detect this signal, with high precision, in 3000 hours, as shown in Figure 5.

Since we only want to detect emission from the IGM, we will need to mask pixels that contain emission from bright galaxies, which for the previously referred resolution would result in $10 - 20\%$ of the pixels being masked. This would not erase much of the information about the filamentary structures (see Sections 4.1 and 6.1 for calculations of the number density of pixels that need to be masked). A higher spatial resolution would, however, easily reduce this masking percentage even more.

Due to the nature of the Ly α line, its FWHM (full-width at half-maximum) will limit the maximum possible resolution of the experiment, or require that galaxy emission is masked from several pixels.

We note that a masking of 20% of the pixels would still allow the recovering of the intensity and power spectra of Lyman alpha emission from the cold IGM, since most of the masked intergalactic gas would correspond to warm/hot gas in the circumgalactic medium.

For the masking of bright galaxies, a complementary experiment would be required. Ideally this can be done with the same spectrometer required to detect the map of the emission from IGM filaments. This is a reasonable assumption, since the only difference necessary for the same experimental setup to be able to detect

these galaxies would be a higher spatial resolution of the order of $1''$ per pixel. This could be achieved with the planned Messier experiment if it had a larger spectral resolution, or with the Multi Unit Spectroscopic Explorer (MUSE) at the VLT if it had a larger field of view and could be extended to lower frequencies (Bacon et al. 2014). Another promising experiment is the World Space Observatory - Ultraviolet (WSO-UV) space telescope, which should be launched in 2021 and aims to detect UV emission in the frequency range corresponding to Ly α emission from $z \sim 0-1.5$ (Boyarchuk et al. 2016). The proposed (WSO-UV) telescope will have the required resolution and sensitivity for detecting both Ly α emission from IGM filaments and from galaxies up to the required flux cut. However, the field of view of this telescope is only $30' \times 30'$ and so not big enough to study IGM filaments at a statistical level.

The technology to detect Ly α emission from the contaminant galaxies thus already exists, but currently none of the proposed experiments meets all the requirements. Alternatively, these galaxies can be detected through their H α emission, since this is a good probe of the galaxies intrinsic Ly α emission. For the relevant frequency range, there are photometric and spectroscopic instruments that can detect galaxies through their H α down to one order of magnitude above the necessary flux limit, or down to $10^{-19} \text{ W m}^{-2}$ in Ly α emission (Sobral et al. 2013).

6 FOREGROUNDS IN LYMAN ALPHA INTENSITY MAPS

Lyman alpha intensity maps will be contaminated by both line and continuum foregrounds. The contamination by line foregrounds can be considerably reduced by masking the pixels contaminated by the most luminous foreground sources, similarly to what was done in Gong et al. (2014) for high redshift Ly α emission. We discuss the line contamination in Ly α intensity maps at $z < 2$ in Section 6.1.

Continuum foregrounds include free-free, free-bound, two photon and UV emission from stars and active galactic nuclei. Most continuum emission can be fitted out of observational maps, since this continuum evolves with frequency more smoothly than the target line emission, which varies according to the emitting structures along the line of sight.

In intensity mapping studies, another important source of radiation is the UV background radiation, which redshifts into the Ly α frequency at the target redshift (Silva et al. 2013; Pullen et al. 2014). Although the photons in the UV background are also continuum emission, if they redshift into the Ly α frequency in a region with a high density of neutral hydrogen, they will scatter in the gas and get re-emitted in a random direction. Therefore, this signal will correlate with the structures in the IGM and will no longer evolve smoothly with frequency. At the low redshifts we are interested in, the probability of a UV photon encountering a region with neutral hydrogen as it redshifts into one of the Lyman-n lines is considerably small, taking into account the highly ionized state of the gas and the small natural width of the Ly α line. We estimate the intensity of this emission as

$$I_{\text{diff cont}}^{\text{Ly}\alpha}(z) = \frac{h\nu_{\text{Ly}\alpha}}{4\pi} \sum_{n=2}^{\infty} f_{\text{rec}}(n) \int_z^{\infty} dz' \frac{c}{(1+z')H(z')} \times \text{SFRD}(z') \epsilon(\nu'_n) P_{\text{abs}}(n, z) \times \prod_{n'=n+1}^{n_{\text{max}}} \{1 - P_{\text{abs}}[n', z_{n'}(z, n)]\}. \quad (12)$$

is taken from Loeb et al. (2005) and modified by Pullen et al. (2014) to account for the case where a fraction of the IGM is ionized. Here $\epsilon(\nu_n)$ is the emissivity rate of a Ly α photon and $f_{\text{rec}(n)}$ accounts for the probability of a Ly α photon to cascade down to a Ly α photon. By using appropriate parameters for the absorption probability (P_{abs}) in the low redshift, highly ionized gas, the resulting scattered emission is extremely low. Our result differs from the high scattering probability found by Pullen et al. (2014), since we determined the optical depth for Ly α absorption with a high resolution simulation instead of using a simplified formula to estimate the probability of neutral hydrogen clumps in the IGM which is not appropriate for the very ionized gas at $z < 2$ where the IGM gas is highly ionized by the strong UV background. We found that, even at $z = 0$, where this scattered Ly α emission should be the highest, our most optimistic values for this emission are of the order of $I_{\text{Ly}\alpha}(z \sim 0) = 10^{-29} \text{ erg s}^{-1} \text{ cm}^{-2} \text{ sr}^{-1} \text{ Hz}^{-1}$. On the other hand, the continuum background at the Ly α frequency will be several orders of magnitude above the proposed signal, see Section 6.2. Therefore, we can consider the UV background as a continuum foreground that evolves smoothly with frequency.

The existence of a strong UV photon source, such as an active galactic nucleus, in the background of a dense gas filament will also produce extended Ly α emission which, depending on its strength, might leave a signature in Ly α intensity maps. The number density of active galactic nuclei is, however, relatively small. Therefore, considering the size of the observational pixel proposed, they can be easily masked without erasing a meaningful fraction of the Ly α signal from the IGM.

An additional complication to the detection of IGM Ly α emission arises from Ly α extended emission around galaxies, typically known as Ly α blobs. The source of power for these large nebulae can vary between energy released during gravitational collapse, star burst activity or active galactic nuclei emission. The failure of GALEX to observe Ly α blobs at $z = 0.8$ indicates that these structures are restricted to high redshifts and so they are not relevant foregrounds for intensity mapping studies at low redshift.

Recent observations of Ly α blobs indicate that these phenomena occur in high density regions and that they are mainly powered by star formation (Ao et al. 2015; Alexander et al. 2016). Given their proximity to star forming regions and AGN, most Ly α blobs will be removed from the observational maps during the galaxy masking. We note that, although the spatial extension of these sources can reach up to 100 kpc, that size is well below the proposed pixel resolution (Yajima et al. 2013).

The Ly α blobs remaining in the observational maps will therefore be subdominant compared to emission from the IGM.

6.1 Line contamination

For the redshift range $z \sim 0-3$, the major line contaminant in Ly α intensity maps is the [OII] 372.2 nm line emission from redshifts $z \sim 0-0.3$, which is observed at the same frequency as Ly α from redshifts $z \sim 2.07-3$.

The OII line luminosity can be estimated with the relation

$$L_{[\text{OII}]} (\text{erg s}^{-1}) = 7.1 \times 10^{40} \text{ SFR} (M_{\odot} \text{ yr}^{-1}) \quad (13)$$

from Kennicutt (1998) and with the SFR parameterization described in Section 3. The resulting OII intensity for $z \sim 0.046$ that will contaminate Ly α intensity maps at $z \sim 2.2$ is $\sim 1.58 \times 10^{-21} \text{ erg s}^{-1} \text{ cm}^{-2} \text{ sr}^{-1}$. We estimated the contamination power spectrum from OII emission scaled to the redshift at which Ly α is

emitted to be approximately two orders of magnitude above the Ly α signal power spectrum at large scales. The required flux cut in the OII emitting galaxies needed to decrease the contamination power spectrum 1 order of magnitude below signal power spectrum is $L_{[\text{OII}]} \sim 1.7 \text{ erg s}^{-1}$. This flux cut corresponds to masking only around 0.09 Mpc^{-3} galaxies. Note that, in the redshift range $2.2 \lesssim z \lesssim 2.06$, where the projection of the contamination power spectra to the redshift of Ly α emission will be particularly high, and so it will be difficult to mask maps in this redshift range. According to this study, the masking percentages required for maps at $z > 2.2$ are smaller than the ones presented at $z = 2.2$.

When it is not possible to spectroscopically observe the contaminant OII galaxies, they can be photometrically observed and distinguished from Ly α emitting galaxies due to the much smaller EW of the OII line (Acquaviva et al. 2014).

6.2 Continuum contamination

Continuum stellar photons emitted with frequencies within the Ly α equivalent width ($\sim 1 \text{ \AA}$) should scatter within the ISM and eventually get re-emitted out of the galaxy as Ly α photons (Jensen et al. 2013). This emission is very weak compared to the nebular Ly α emission and can therefore be safely neglected.

However, continuum stellar emission below and above the Ly α frequency will, contaminate Ly α intensity maps. We estimate this contamination by assuming that the number of photons emitted by a galaxy within the relevant frequency range follows the spectrum of a black body with an average temperature of $\sim 2.2 \times 10^4 \text{ K}$. We estimate, the black body temperature at each emitted frequency by averaging over a Salpeter stellar mass function, the temperature of the stars weighted by the lifetime of their nuclear phase and by their relative emissivity at the relevant frequency range.

The galaxy spectrum, amplitude was set, assuming that the average relation between the galaxy SFR and its luminosity in the range $1500 \text{ \AA} < \lambda < 2800 \text{ \AA}$ follows the relation

$$\frac{\text{SFRD}(z)}{[\text{M}_{\odot} \text{ yr}^{-1} \text{ Mpc}^{-3}]} = 1.05 \times 10^{-28} \frac{\rho_{\text{UV}}}{[\text{erg s}^{-1} \text{ Mpc}^{-3} \text{ Hz}^{-1}]}, \quad (14)$$

where ρ_{UV} is the galaxies luminosity density (Haardt & Madau 2012). The continuum stellar intensity at the observed frequency is

$$I_{\nu_o}^{\text{stellar}}(z_{\text{Ly}\alpha}) = A \int_{\nu_{\text{min}}}^{\nu_{\text{max}}} d\nu \frac{h\nu^3}{e^{h\nu/k_{\text{B}}T_{\text{K}}} - 1} \times \frac{\text{SFRD}(z)y(z)}{4\pi(1+z)^2} f_{\text{esc}}^{\text{UV}}, \quad (15)$$

where $A = 4.19 \times 10^9$ sets the number of UV photons estimated with the black body approximation to follow the relation presented in equation 14. Here, ν_o is the frequency at which the Lyman alpha line is observed when emitted from the redshift $z_{\text{Ly}\alpha}$, $\nu = \nu_o(1+z)$ is the emitted frequency and $f_{\text{esc}}^{\text{UV}}$ is the fraction of the emitted UV photons that escape the galaxy without being absorbed by dust. We integrate the continuum emission from $\nu_{\text{min}} = \nu_{\text{Ly}\alpha}/(1+z_{\text{Ly}\alpha})$ to $\nu_{\text{max}} = 7.4 \times 10^{15} \text{ Hz}$, which corresponds to photons with energies 30.6 eV . For most stars the radiation released above this energy is very small, so our results are not very sensitive to the choice of ν_{max} .

We parameterize the escape fraction of UV photons below the Lyman alpha frequency as $f_{\text{esc}}^{\text{UV}} = 10^{-0.4A(\nu, z)k(\nu)}$ and, following

Haardt & Madau (2012), we take the magnitude of the attenuation to be:

$$A(\nu, z) = A_{\text{FUV}} \frac{k(\nu)}{k(1500 \text{ \AA})}, \quad (16)$$

where

$$A_{\text{FUV}}(z) = \begin{cases} 1 & (0 \leq z \leq 2); \\ 2.5 \log[(1 + 1.5/(z - 1))] & (z > 2). \end{cases} \quad (17)$$

To scale the attenuation with frequency we use the starburst reddening curve, $k(\nu)$, from Calzetti et al. (2000).

We take $f_{\text{esc}}^{\text{UV}} = 0.3$ for emission between the Ly α and the Lyman limit frequencies and $f_{\text{esc}}^{\text{UV}} = 0.2$ for ionizing UV emission (following the study by Yajima et al. (2014)). Given the uncertainty in the escape fraction of photons above the Ly α frequency, a lower limit for this intensity can be obtained by setting $z_{\text{max}} = z_{\text{Ly}\alpha}$.

Additional free-free, free-bound and two-photon radiation emitted from redshifts below the Ly α target redshift will also contribute to the ultraviolet background radiation. Free-free and free-bound emission is, respectively, originated when free electrons scatter off ions with or without being captured. The intensity of free-free and free-bound radiation can be modeled as:

$$I_{\nu_o}^{\text{free}}(z_{\text{Ly}\alpha}) = \int_{\nu_{\text{min}}}^{\nu_{\text{max}}} d\nu f_{\text{volume}}(z) \frac{\varepsilon_{\nu}}{4\pi(1+z)^2} y(z), \quad (18)$$

where ε_{ν} is the total volume emissivity (which we estimated as in (Dopita & Sutherland 2003)) and f_{volume} is the volume fraction of the Universe which contains free electrons and ions.

At the relevant redshift range most of the gas in the IGM is ionized. However, for estimating f_{volume} it is useful to divide the IGM in three regions which have very different astrophysical properties. The CGM, which is very dense ($\delta > 100$), has a temperature of $T_{\text{K}} \sim 10^5 \text{ K}$ and contains around 5% of the baryons. The IGM gas filaments, with overdensities in the range $1 > \delta > 180$ has a temperature of $T_{\text{K}} \sim 10^4 \text{ K}$ and contains more than 40% of the baryons. Finally, we consider the voids. These are characterized by overdensities of $\delta < 1$ and only contain a small fraction of the baryons in the Universe. Given the low luminosities involved, it is safe to neglect emission from voids. Therefore, we estimate the volume fraction of the IGM emitting continuum radiation as the volume occupied by filaments, which is around 5% of the total volume in our simulations, in agreement with the results from N-body simulations and from the SDSS detected filaments analyzed by Tempel et al. (2014).

To estimate free-free and free-bound emission from filaments, it is a good approximation to assume that all of the gas is ionized and that it has a clumping factor of $C \sim 5$ (value estimated from our simulations). The volume emissivity estimated by Dopita & Sutherland (2003) is given by:

$$\varepsilon_{\nu} = 10^{8.1} C n_e n_p \gamma_c \frac{e^{-h\nu/k_{\text{B}}T_{\text{K}}}}{T_{\text{K}}^{1/2}} \text{ erg cm}^{-3} \text{ s}^{-1} \text{ Hz}^{-1}, \quad (19)$$

where γ_c is the continuum emission coefficient, including free-free and free-bound emission given, in SI units by:

$$\gamma_c = 5.44 \times 10^{-46} \left[\bar{g}_{\text{ff}} + \sum_{n=n'}^{\infty} \frac{x_n e^{x_n}}{n} g_{\text{fb}}(n) \right]. \quad (20)$$

Here, $x_n = Ry/(k_{\text{B}}T_{\text{K}}n^2)$, where k_{B} is the Boltzmann constant, n is the level to which the electron recombines, $Ry = 13.6 \text{ eV}$

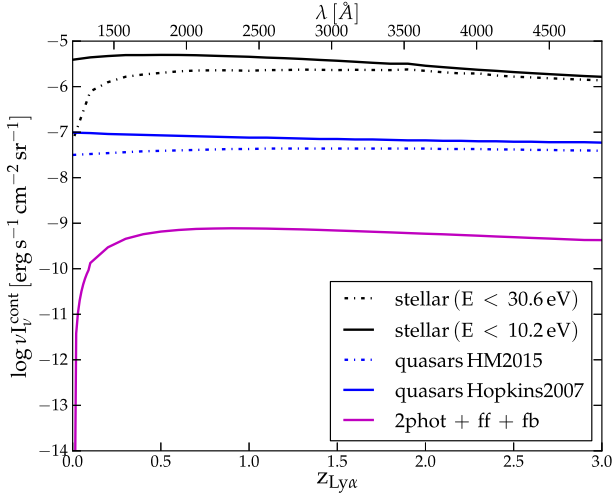


Figure 7. Intensity of continuum background contamination in Lyman alpha intensity maps as a function of the Lyman alpha emission redshift. The black lines denote the predicted intensity from stellar UV emission. The upper black solid line includes UV emission below 30.6 eV, while the lower black solid line only includes UV emission below 10.2 eV. The blue lines account for quasar emission according to the Hopkins et al. (2007) and the Madau & Haardt (2015) models. The magenta line includes continuum contamination from 2-photon, free-free and free-bound emission.

and $\bar{g}_{ff} \approx 1.1 - 1.2$ and $g_{fb}(n) \approx 1.05 - 1.09$ are the thermally average Gaunt factors for free-free and free-bound emission, respectively, (Karzas & Latter 1961). The initial level n' is set by the condition $cR_\infty/n'^2 < \nu < cR_\infty/(n' - 1)^2$, where $R_\infty = 1.1 \times 10^7 \text{ m}^{-1}$ is the Rydberg constant. In an ionized gas, the number density of protons is $n_p = n_H + 2n_{\text{He}}$ and the number density of electrons is $n_e = n_H + 2n_{\text{He}}$.

The average number densities in the filaments from the simulation are therefore $n_H = \frac{0.4}{0.05} (1 - Y_p) \bar{n}_b \sim 1.49 \times 10^{-6} \text{ cm}^{-3}$ and $n_{\text{He}} = \frac{0.4}{0.05} Y_p \bar{n}_b / 4 \sim 1.23 \times 10^{-7} \text{ cm}^{-3}$, where \bar{n}_b is the baryon number density. Similarly, during a recombination, there is a probability of two photons being emitted.

The observed intensity due to 2-photon emission is

$$\begin{aligned} I_{\nu_o}^{2\text{-photon}}(z_{\text{Ly}\alpha}) &= C n_e n_p \alpha_A (1 - f_{\text{Ly}\alpha}) \\ &\times \int_{\nu_{\text{min}}}^{\nu_{\text{Ly}\alpha}} d\nu \frac{2h\nu}{\nu_{\text{Ly}\alpha}} \frac{P(\nu/\nu_{\text{Ly}\alpha})}{4\pi} \\ &\times (1+z)y(z), \end{aligned} \quad (21)$$

where $P(y)dy$ is the normalized probability that, in a two photon decay, one of them is in the range $dy = d\nu/\nu_{\text{Ly}\alpha}$. The factor $1 - f_{\text{Ly}\alpha} \approx 1/3$ accounts for the probability of 2-photon emission during a hydrogen recombination. This probability was fitted by Fernandez & Komatsu (2006), using Table 4 of Brown & Mathews (1970), as:

$$\begin{aligned} P(y) &= 1.307 - 2.627(y - 0.5)^2 + 2.563(y - 0.5)^4 \\ &- 51.69(y - 0.5)^6. \end{aligned} \quad (22)$$

The last missing contribution to the UV continuum background is emission from active galactic nuclei which we modeled using, as a lower limit, the quasar comoving emissivity at 1 ryd from Hopkins et al. (2007), fitted by Haardt & Madau (2012) as:

$$\begin{aligned} \frac{\epsilon_{912}(z)}{(1+z)^3} &= (10^{24.6} \text{ erg s}^{-1} \text{ Mpc}^{-3} \text{ Hz}^{-1}) \\ &\times (1+z)^{4.68} \frac{\exp(-0.28z)}{\exp(1.77z) + 26.3}. \end{aligned} \quad (23)$$

The emissivity scales with $\nu^{-0.44}$ for ($\lambda > 1300\text{\AA}$) and with $\nu^{-1.57}$ for ($\lambda < 1300\text{\AA}$), as observed in the spectra of radio quiet sources (Vanden Berk et al. 2001; Telfer et al. 2002). An upper limit to this emissivity can be obtained with the Madau & Haardt (2015) model, derived from fits to several observational data sets. This upper limit is given by:

$$\log \epsilon_{912}(z) = 25.15e^{-0.0026z} - 1.5e^{-1.3z}. \quad (24)$$

and scales with frequency as $\nu^{-0.61}$ Lusso et al. (2015).

The quasar luminosity density contributing to the UV background at the observed Ly α frequency is

$$I_{\nu_o}^{\text{quasar}}(z_{\text{Ly}\alpha}) = 10^{-73.468} \int_{\nu_{\text{min}}}^{\nu_{\text{max}}} d\nu \frac{\epsilon_\nu y(z)}{4\pi(1+z)^5}, \quad (25)$$

where $\nu_{\text{max}} = 6.0 \times \nu_o$. Note that the bulk of this emission originates at redshifts very close to $z_{\text{Ly}\alpha}$ or at lower redshifts. Therefore, the result is not very sensitive to the choice of ν_{max} .

As observed in Figure 7, the intensity of continuum contamination in Ly α intensity maps is higher than the intensity of Ly α emission from filaments. The former intensity is, however, quite uncertain, with model predictions differing by over one order of magnitude (Domínguez et al. 2011). Therefore, constraining this extragalactic background (continuum) light (EBL) is one of the objectives of the proposed experiment. Since the SFR model we take as reference is well within current constraints, we believe that the difference in the predicted EBL originates in the uncertainty in the quasars UV emissivity. This further supports the need to detect the effects of this UV continuum in the IGM, so that we can better constrain it.

The intensity of contamination found is compatible with the predicted evolution of the EBL from Domínguez et al. (2011) if we assume that the escape fraction of photons with frequencies above the Ly α line is very small. This would result in the contamination given by the black dashed dotted line in Figure 7. Our model can also easily fit the observational constraints from Gardner et al. (2000) and from Xu et al. (2005) for different assumptions about the photon escape fraction.

However, the smoothness of this foreground across frequency, compared to the Ly α signal, should allow it to be fitted and removed from the observational maps in the same manner as the foregrounds for 21 cm line intensity maps are removed (e.g. Wang et al. 2006). This fitted foreground can, in principle, be used to probe the EBL.

7 CONCLUSIONS

Mapping gas filaments in the IGM is an essential step to complete our picture of the spatial distribution of large scale structures throughout the Universe. These maps can provide much more information about the baryonic matter spatial distribution than observing emission from galaxies, which are just discrete point sources in the point of view of large scale studies.

Cold IGM filaments can only be directly detected through emission lines from hydrogen or helium. Therefore, this study explores the prospects for detecting and mapping hydrogen Ly α emission from IGM filaments at $z < 3$.

In this redshift range the Ly α line is mostly observed in the UV band and, according to our conservative predictions, the Ly α signal from cold IGM filaments can be detected by an experiment with a sensitivity of $3.7 \times 10^{-9} \text{ erg s}^{-1} \text{ cm}^{-2} \text{ sr}^{-1}$ ($\sim 37 \text{ mag/arcsec}^2$) in the UV band, which is in the reach of the next generation satellites. The Ly α emission from these filaments is powered by the UV background and, in most cases, will emit with a maximum intensity of about half the intensity of the UV background. It can therefore be used to probe and constrain this poorly constrained background.

Emission in the Ly α line from filaments can be used to probe the baryonic content of the IGM, as well as the thermal and ionization state of these baryons. Intensity mapping of IGM filaments with two emission lines, such as the HI Ly α and the HI 21 cm line, will allow for even better constraints to the astrophysical conditions in filaments. This is essential to properly model the gas flow between galaxies and the IGM.

In this study, we consider the continuum foregrounds that will contaminate Ly α intensity maps and find that a mission with the experimental setup that we here propose has the required sensitivity to map the proposed signal and enough angular and frequency resolution to be able to remove the main line foregrounds and continuum foregrounds.

ACKNOWLEDGEMENTS

We thank the Netherlands Foundation for Scientific Research support through the VICI grant 639.043.006.

REFERENCES

- Acquaviva V., Gawiser E., Leung A. S., Martin M. R., 2014, in IAU Symposium, Vol. 306, Statistical Challenges in 21st Century Cosmology, Heavens A., Starck J.-L., Krone-Martins A., eds., pp. 365–368
- Alexander D. M., Simpson J. M., Harrison C. M., Mullaney J. R., Smail I., Geach J. E., Hickox R. C., Hine N. K., Karim A., Kubo M., Lehmer B. D., Matsuda Y., Rosario D. J., Stanley F., Swinbank A. M., Umehata H., Yamada T., 2016, ArXiv e-prints
- Ao Y., Matsuda Y., Beelen A., Henkel C., Cen R., De Breuck C., Francis P. J., Kovács A., Lagache G., Lehnert M., Mao M. Y., Menten K. M., Norris R. P., Omont A., Tatemastu K., Weiß A., Zheng Z., 2015, *A&A*, 581, A132
- Bacon R., Vernet J., Borisova E., Bouché N., Brinchmann J., Carollo M., Carton D., Caruana J., Cerda S., Contini T., Franx M., Girard M., Guerou A., Haddad N., Hau G., Herenz C., Herrera J. C., Husemann B., Husser T.-O., Jarno A., Kamann S., Krajinovic D., Lilly S., Mainieri V., Martinsson T., Palsa R., Patricio V., Pécontal A., Pello R., Piqueras L., Richard J., Sandin C., Schroetter I., Selman F., Shirazi M., Smette A., Soto K., Streicher O., Urrutia T., Weillbacher P., Wisotzki L., Zins G., 2014, *The Messenger*, 157, 13
- Becker G. D., Bolton J. S., Haehnelt M. G., Sargent W. L. W., 2011, *MNRAS*, 410, 1096
- Behroozi P. S., Wechsler R. H., Conroy C., 2013, *ApJ*, 770, 57
- Boyarchuk A. A., Shustov B. M., Savanov I. S., Sachkov M. E., Bisikalo D. V., Mashonkina L. I., Wiebe D. Z., Schematovich V. I., Shchekinov Y. A., Ryabchikova T. A., Chugai N. N., Ivanov P. B., Voshchinnikov N. V., Gomez de Castro A. I., Lamzin S. A., Piskunov N., Ayres T., Strassmeier K. G., Jeffrey S., Zwintz S. K., Shulyak D., Gérard J.-C., Hubert B., Fossati L., Lammer H., Werner K., Zhilkin A. G., Kaigorodov P. V., Sichevskii S. G., Ustamaich S., Kanev E. N., Kil'pio E. Y., 2016, *Astronomy Reports*, 60, 1
- Boylan-Kolchin M., Springel V., White S. D. M., Jenkins A., Lemson G., 2009, *MNRAS*, 398, 1150
- Calzetti D., Armus L., Bohlin R. C., Kinney A. L., Koornneef J., Storchi-Bergmann T., 2000, *ApJ*, 533, 682
- Cantalupo S., Arrigoni-Battaia F., Prochaska J. X., Hennawi J. F., Madau P., 2014, *Nature*, 506, 63
- Davé R., Oppenheimer B. D., Katz N., Kollmeier J. A., Weinberg D. H., 2010, *MNRAS*, 408, 2051
- De Lucia G., Blaizot J., 2007, *MNRAS*, 375, 2
- Dijkstra M., 2014, *PASA*, 31, 40
- Dijkstra M., Jeason-Daniel A., 2013, *MNRAS*, 435, 3333
- Domínguez A., Primack J. R., Rosario D. J., Prada F., Gilmore R. C., Faber S. M., Koo D. C., Somerville R. S., Pérez-Torres M. A., Pérez-González P., Huang J.-S., Davis M., Guhathakurta P., Barmby P., Conselice C. J., Lozano M., Newman J. A., Cooper M. C., 2011, *MNRAS*, 410, 2556
- Dopita M. A., Sutherland R. S., 2003, *Astrophysics of the diffuse universe*
- Fernandez E. R., Komatsu E., 2006, *ApJ*, 646, 703
- France K., Hoadley K., Fleming B. T., Kane R., Nell N., Beasley M., Green J. C., 2015, ArXiv e-prints
- Fukugita M., Kawasaki M., 1994, *MNRAS*, 269, 563
- Furlanetto S. R., Schaye J., Springel V., Hernquist L., 2003, *ApJL*, 599, L1
- , 2004, *ApJ*, 606, 221
- , 2005, *ApJ*, 622, 7
- Gardner J. P., Brown T. M., Ferguson H. C., 2000, *ApJL*, 542, L79
- Gong Y., Silva M., Cooray A., Santos M. G., 2014, *ApJ*, 785, 72
- Gould A., Weinberg D. H., 1996, *ApJ*, 468, 462
- Green J. C., Wilkinson E., Morse J. A., 2003, in *Proc. SPIE, Vol. 4854, Future EUV/UV and Visible Space Astrophysics Missions and Instrumentation*, Blades J. C., Siegmund O. H. W., eds., pp. 72–80
- Gunn J. E., Peterson B. A., 1965, *ApJ*, 142, 1633
- Guo Q., White S., Boylan-Kolchin M., De Lucia G., Kauffmann G., Lemson G., Li C., Springel V., Weinmann S., 2011, *MNRAS*, 413, 101
- Haardt F., Madau P., 2012, *ApJ*, 746, 125
- Hayes M., Schaerer D., Östlin G., Mas-Hesse J. M., Atek H., Kunth D., 2011, *ApJ*, 730, 8
- Hopkins P. F., Richards G. T., Hernquist L., 2007, *ApJ*, 654, 731
- Jensen H., Laursen P., Mellema G., Iliev I. T., Sommer-Larsen J., Shapiro P. R., 2013, *MNRAS*, 428, 1366
- Karzas W. J., Latter R., 1961, *ApJS*, 6, 167
- Keating L. C., Haehnelt M. G., Becker G. D., Bolton J. S., 2014, *MNRAS*, 438, 1820
- Keel W. C., White III R. E., Chapman S., Windhorst R. A., 2009, *AJ*, 138, 986
- Kennicutt Jr. R. C., 1998, *ApJ*, 498, 541
- Kollmeier J. A., Zheng Z., Davé R., Gould A., Katz N., Miralda-Escudé J., Weinberg D. H., 2010, *ApJ*, 708, 1048
- Liang C. J., Kravtsov A. V., Agertz O., 2015, ArXiv e-prints
- Lidz A., Faucher-Giguère C.-A., Dall’Aglia A., McQuinn M., Fechner C., Zaldarriaga M., Hernquist L., Dutta S., 2010, *ApJ*, 718, 199
- Loeb A., Barkana R., Hernquist L., 2005, *ApJ*, 620, 553
- Lusso E., Worsecck G., Hennawi J. F., Prochaska J. X., Vignali C., Stern J., O’Meara J. M., 2015, *MNRAS*, 449, 4204

- Madau P., Haardt F., 2015, *ApJL*, 813, L8
- Maraston C., 2005, *MNRAS*, 362, 799
- Martin D. C., Chang D., Matuszewski M., Morrissey P., Rahman S., Moore A., Steidel C. C., 2014, *ApJ*, 786, 106
- Meiksin A. A., 2009, *Reviews of Modern Physics*, 81, 1405
- Morse J. A., Green J. C., Ebbets D. C., Andrews J. P., Heap S. R., Leitherer C., Linsky J. L., Savage B. D., Shull J. M., Snow T. P., Stern S. A., Stocke J. T., Wilkinson E., 1998, in *Proc. SPIE*, Vol. 3356, *Space Telescopes and Instruments V*, Bely P. Y., Breckinridge J. B., eds., pp. 361–368
- Oke J. B., Gunn J. E., 1983, *ApJ*, 266, 713
- Planck Collaboration, Ade P. A. R., Aghanim N., Armitage-Caplan C., Arnaud M., Ashdown M., Atrio-Barandela F., Aumont J., Baccigalupi C., Banday A. J., et al., 2014, *A&A*, 571, A16
- Popping G., Caputi K. I., Trager S. C., Somerville R. S., Dekel A., Kassin S. A., Kocevski D. D., Koekemoer A. M., Faber S. M., Ferguson H. C., Galametz A., Grogan N. A., Guo Y., Lu Y., Wel A. v. d., Weiner B. J., 2015, *MNRAS*, 454, 2258
- Pullen A. R., Doré O., Bock J., 2014, *ApJ*, 786, 111
- Santos M. G., Ferramacho L., Silva M. B., Amblard A., Cooray A., 2010, *MNRAS*, 406, 2421
- Schaye J., Theuns T., Rauch M., Efstathiou G., Sargent W. L. W., 2000, *MNRAS*, 318, 817
- Shull J. M., Harness A., Trenti M., Smith B. D., 2012, *ApJ*, 747, 100
- Silva M., Santos M. G., Gong Y., Cooray A., 2012, *ArXiv e-prints*
- Silva M. B., Santos M. G., Gong Y., Cooray A., Bock J., 2013, *ApJ*, 763, 132
- Sobral D., Smail I., Best P. N., Geach J. E., Matsuda Y., Stott J. P., Cirasuolo M., Kurk J., 2013, *MNRAS*, 428, 1128
- Springel V., 2005, *MNRAS*, 364, 1105
- Springel V., White S. D. M., Jenkins A., Frenk C. S., Yoshida N., Gao L., Navarro J., Thacker R., Croton D., Helly J., Peacock J. A., Cole S., Thomas P., Couchman H., Evrard A., Colberg J., Pearce F., 2005, *Nature*, 435, 629
- Springel V., Yoshida N., White S. M., 2001, *New Astronomy*, 6, 79
- Telfer R. C., Zheng W., Kriss G. A., Davidsen A. F., 2002, *ApJ*, 565, 773
- Tempel E., Stoica R. S., Martínez V. J., Liivamägi L. J., Castellan G., Saar E., 2014, *MNRAS*, 438, 3465
- Tuttle S. E., Schiminovich D., Matuszewski M., Rahman S., McLean R., Martin C., Frank S., Milliard B., Deharveng J., 2010, in *Bulletin of the American Astronomical Society*, Vol. 42, *American Astronomical Society Meeting Abstracts #215*, p. 316
- Vanden Berk D. E., Richards G. T., Bauer A., Strauss M. A., Schneider D. P., Heckman T. M., York D. G., Hall P. B., Fan X., Knapp G. R., Anderson S. F., Annis J., Bahcall N. A., Bernardi M., Briggs J. W., Brinkmann J., Brunner R., Burles S., Carey L., Castander F. J., Connolly A. J., Crocker J. H., Csabai I., Doi M., Finkbeiner D., Friedman S., Frieman J. A., Fukugita M., Gunn J. E., Hennessy G. S., Ivezić Ž., Kent S., Kunszt P. Z., Lamb D. Q., Leger R. F., Long D. C., Loveday J., Lupton R. H., Meiksin A., Merelli A., Munn J. A., Newberg H. J., Newcomb M., Nichol R. C., Owen R., Pier J. R., Pope A., Rockosi C. M., Schlegel D. J., Siegmund W. A., Smees S., Snir Y., Stoughton C., Stubbs C., SubbaRao M., Szalay A. S., Szokoly G. P., Tremonti C., Uomoto A., Waddell P., Yanny B., Zheng W., 2001, *AJ*, 122, 549
- Wang X., Tegmark M., Santos M. G., Knox L., 2006, *ApJ*, 650, 529
- Xu C. K., Donas J., Arnouts S., Wyder T. K., Seibert M., Iglesias-Páramo J., Blaizot J., Small T., Milliard B., Schiminovich D., Martin D. C., Barlow T. A., Bianchi L., Byun Y.-I., Forster K., Friedman P. G., Heckman T. M., Jelinsky P. N., Lee Y.-W., Madore B. F., Malina R. F., Morrissey P., Neff S. G., Rich R. M., Siegmund O. H. W., Szalay A. S., Welsh B. Y., 2005, *ApJL*, 619, L11
- Yajima H., Li Y., Zhu Q., 2013, *ApJ*, 773, 151
- Yajima H., Li Y., Zhu Q., Abel T., Gronwall C., Ciardullo R., 2014, *MNRAS*, 440, 776